Zitierweise: *Angew. Chem. Int. Ed.* **2023**, *62*, e202303081
doi.org/10.1002/anie.202303081

Thermal Conductivity

Maldistribution of Chemical Bond Strength Inducing Exceptional Anisotropy of Thermal Conductivity in Non-Layered Materials

Yang Hua[+], Wei Bai[+], Shengnan Dai[+], Rongjie He[+], Pengfei Nan[+], Liang Sun, Jiong Yang, Bo Sun,* Binghui Ge,* Chong Xiao,* and Yi Xie*

Abstract: Currently, the efforts to find materials with high κ anisotropy ratios mainly focus on layered materials, however, the limited quantity and lower workability comparing to non-layered ones boost the exploration of non-layered materials with high κ anisotropy ratios. Here, taking $PbSnS_3$, a typical non-layered orthorhombic compound, as an example, we propose that maldistribution of chemical bond strength can lead to large anisotropy of κ in non-layered materials. Our result reveals that the maldistribution of Pb–S bonds lead to obvious collective vibrations of dioctahedron chain units, resulting in an anisotropy ratio up to 7.1 at 200 K and 5.5 at 300 K, respectively, which is one of the highest ever reported in non-layered materials and even surpasses many classical layered materials such as Bi_2Te_3 and SnSe. Our findings can not only broaden the horizon for exploring high anisotropic κ materials but also provide new opportunities for the application of thermal management.

Introduction

As one important characteristic attribute of matter, anisotropy is the focus of condensed matter physics, solid chemistry, crystallography, and materials science. The anisotropy of material should unexpectedly endow it novel physical properties, which brings a revolutionary not only in science and technology but also in our daily life, such as magnetocrystalline anisotropy,[1–4] two-dimensional superconductivity,[5] two-dimensional electron/hole gas,[6–8] anisotropic magneto-Peltier effect,[9] anisotropic Gilbert damping,[10] anisotropic spin fluctuations,[11] anisotropic excitons,[12] anisotropy-boosted transverse thermoelectricity,[13] and anisotropic van der Waals (vdW) thermal conductors.[14] Therefore, the ability to design and control the anisotropy of physical properties becomes key prerequisite for many modern functional materials.

The most effective approach of realizing macroscopic anisotropy is to design chemical bonds strategically, as chemical bonds are the primary drivers of material properties. The directionality as well as the strength distribution of chemical bonds can play a critical role in determining the anisotropic behavior of materials. For instance, materials that have covalent bonding tend to have highly directional bonds, which can lead to strong anisotropy in their physical properties, while materials with metallic bonding tend to have more delocalized electrons, which can result in weaker anisotropy. Similarly, in polymers, the orientation of the polymer chains and the distribution of hydrogen bonds can lead to anisotropic stiffness when stretched along or perpendicular to the direction of the polymer chains.

In crystalline materials, layered materials exhibit distinct inter- and intra-layer forces that create a spatially non-uniform distribution of chemical bond strength. These forces, which can include electrostatic or hydrogen bonding in addition to weak van der Waals interactions, result in a significant anisotropy in the material's properties. As a result, layered materials are often used as prototypes to study large anisotropic behaviors such as electricity, magnet-

[*] Y. Hua,[+] Dr. W. Bai,[+] L. Sun, Prof. C. Xiao, Prof. Y. Xie
Hefei National Research Center for Physical Sciences at the Microscale, University of Science and Technology of China
230026 Hefei, Anhui (P. R. China)
E-mail: cxiao@ustc.edu.cn

Dr. W. Bai,[+] Prof. C. Xiao, Prof. Y. Xie
Institute of Energy, Hefei Comprehensive National Science Center
230031 Hefei, Anhui (P. R. China)

S. Dai,[+] Prof. J. Yang
Materials Genome Institute, Shanghai University
200444 Shanghai (P. R. China)
E-mail: jiongy@t.shu.edu.cn

R. He,[+] Prof. B. Sun
Tsinghua-Berkeley Shenzhen Institute, Tsinghua University
518055 Shenzhen, Guangdong (P. R. China)
E-mail: sun.bo@sz.tsinghua.edu.cn

Prof. B. Sun
Institute of Material Research, Tsinghua Shenzhen International Graduate School, Guangdong Provincial Key Laboratory of Thermal Management Engineering and Materials, Tsinghua University
518055 Shenzhen, Guangdong, (P. R. China)

Dr. P. Nan,[+] Prof. B. Ge
Information Materials and Intelligent Sensing Laboratory of Anhui Province, Institutes of Physical Science and Information Technology, Anhui University
230601 Hefei, Anhui (P. R. China)
E-mail: bhge@ahu.edu.cn

Prof. C. Xiao
Dalian National Laboratory for Clean Energy, Chinese Academy of Science
116023 Dalian, Liaoning (P. R. China)

[+] These authors contributed equally to this work.

ism, optics, and mechanics and have played an important role in the modern information society. However, unfortunately, the industrial processing of large-scale layered materials is not as mature as that of non-layered materials, posing challenges along the road to commercialization. Meanwhile, materials with layered characteristics only account for about a twentieth of all bulk materials in the crystal database, which means much more materials with potential performance have crystal structures in three rather than two dimensions. Therefore, quite sensibly, non-layered materials provide more opportunities to observe excellent characteristics and there will be a lot of prospects if we can explore high anisotropy beyond the consequence of vdW interactions.

The thermal conductivity (κ) is a key parameter in thermal management field[15] such as thermoelectric energy conversion,[16] silica glass for everyday thermal insulation and thermal barrier coatings of metal components in gas-turbine or diesel engines.[17] For example, anisotropic thermal conductors, in which heat flows faster in one direction than in the other, can rapidly remove heat from local overheating hotspots in the directions with high κ and simultaneously provide thermal insulation along the slow thermal diffusion axis,[14,18] is an indispensable cooling mode in densified integrated circuits.[19–21] The fibers with anisotropic κ can be shaped into flexible and inexpensive polymer sheets for textile clothing with the integrated abilities of ventilation and insulation.[22–25] Therefore, considering the wide outlook of processing industry and commerce, the study of functional materials with high κ anisotropy ratios can provide important guidance on special thermal management situation. In fact, the technological progress of developing large anisotropic thermal conductivity is evolving continuously with a large worldwide effort in human and monetary capital. Recently, J. Park et al. reported a method to prepare large area anisotropic thermal conductors by using random rotation between crystal layers with extremely thermal anisotropy ratio in vdW compound.[14] However, so far, the anisotropy ratio of thermal conductivity in non-layered materials is almost rarely large than 2. Therefore, there will be a lot of prospects if we can explore high thermal anisotropy in non-layered materials beyond the consequence of vdW gap in layered materials.

In order to obtain large anisotropic κ in non-layered materials, we trace to the differences between layered materials and non-layered materials. In the layered materials, each layer is connected by ionic/covalent bonds and separated by weak vdW forces, so that the separated independent layer can be treated as a whole rigid ball with two distinct phonon modes of collective vibration—the shear and breathing modes—which usually does not occur in non-layered materials due to the absence of the vdW gaps.[26,27] These two types of collective vibrations are usually accompanied by the anisotropy of sound velocity, inducing obvious anisotropic κ. Consequently, it provides perspective insight if we can introduce a separated vibration entirety similar to layered compounds without destroying the structure of non-layered materials, it should be hopeful to obtain a large anisotropy κ ratio in non-layered materials. Inspired by this, some non-layered materials with maldistribution of chemical bond strength attracted our attention where atoms connected by strong bonds form integral units, and these units connect with each other by weaker bonds, similar to the slab in layered compounds. Therefore, it is reasonable to believe that this maldistribution of chemical bond strength provides a good platform for us to obtain large anisotropic κ in non-layered compounds.

Herein, we take non-layered $PbSnS_3$, which crystalizes as orthorhombic structures and belongs to Pnma space group,[28,29] as an example to explore the large anisotropy induced by maldistribution of chemical bond strength. We discovered an anisotropy ratio of κ up to 7.1 at 200 K (and 5.5 at 300 K) which is extremely large among non-layered materials and can even surpasses some classical layered materials with vdW gaps such as Bi_2Te_3 and SnSe. Due to the 6 s lone pair electrons of Pb atoms, there is a kind of intermediate strength Pb–S bonds in $PbSnS_3$ of which the interaction is weaker than ordinary covalent bond/ionic bonds but stronger than vdW force. The maldistribution of Pb–S bonds strength splits $PbSnS_3$ into quasi-independent dioctahedron chains, leading to the collective vibration and anisotropic sound velocity, which endows $PbSnS_3$ with large anisotropic κ. The maldistribution of chemical bond strength can shed light on exploring the high thermal anisotropic materials and provide worthy experience for applications of thermal management.[30]

Results and Discussion

The single crystals $PbSnS_3$ were synthesized by solid sintering (photograph of single crystals in Figure S1, elemental analysis in Figure S2, the single-crystal crystallographic data and refinement details in Table S1 and S2). In $PbSnS_3$, the Sn atoms bonds with the S atoms to form $[SnS_6]$ octahedra (lilac in Figure 1a), while the Pb atoms form trigonal pyramidal coordination with S atoms due to lone pair 6 s electrons of Pb atoms, which are located at the bottom of the second occupied valence subband (Figure S3), pointed to the depth of void formed by sulfur atoms in adjacent chains (Figure 1b) and repel the angle of intra-unit S–Pb–S being less than 109°48′ (Figure S4). Two Pb-capped $[SnS_6]$ octahedra form a unit through edge-sharing, which infinitely grow along *b* axis to form a dioctahedron chain. In this dioctahedron chain, the length of Pb–S and Sn–S bonds is about 2.7–2.9 Å and 2.5–2.6 Å respectively, which belong to typical hybrid of covalent bonds and ionic bonds (Figure 1c). While between two adjacent dioctahedron chain, the distance between Pb and the nearest S atom in the adjacent chain is ≈3.1 Å, which is farther apart than the covalent bonds inside the double octahedron chain but shorter than the sum of Pb and S vdW radii ≈3.8 Å. Furthermore, the evaluation of Crystal Orbital Hamilton Populations (COHP) proves that the strength of intra-unit Pb–S bonds are much stronger than that of inter-unit bonds due to the relatively larger bonding contributions of valence electrons over anti-bonding contributions, although the integrated COHP (ICOHP) of inter-unit Pb–S interactions

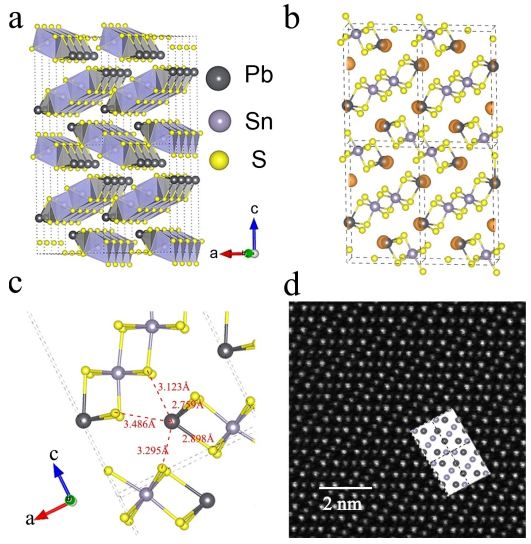

Figure 1. The maldistribution of chemical bond strength in $PbSnS_3$. a) Schematic of the coordination structure. b) The electron localization function. The localized Pb 6s lone pairs (brown) spatially point to the depth of void formed by sulfur atoms in adjacent chains. c) The length of Pb–S bonds inside the dioctahedron-chain unit and three nearest distances between neighbored units. d) The HAADF-STEM image of *ac* plane. 2×2 cells atomic model arrangement is inserted.

are also negative (Figure S5). The COHP is a tool used for analyzing the bonding between two atoms in a solid, which is calculated by multiplying the density of states (DOS) with the Hamiltonian matrix element of the interaction between the orbitals of neighboring atoms. It reflects the contributions of the bonding term (which lowers the total energy) and the antibonding term (which raises the total energy) to the energy of the band structure. Meanwhile, the ICOHP method is used to analyze the total bonding between two atoms in a solid, which is achieved by integrating the part of the COHP below the Fermi level, and can be used to evaluate the strength of covalent bonds in the crystal. In $PbSnS_3$, the ICOHP for the Pb–S bonds between chain unit is significantly smaller than that within a chain unit. These results show that the lone pair 6 s electrons of Pb atoms endow $PbSnS_3$ with a very unique structural feature of maldistributed chemical bond strength, i.e., there is a strong covalent/ionic bond connection inside the dioctahedron chains, while the interaction between the dioctahedron is relatively weak, similar to the contrast of the interaction strength between the intra-layers and the inter-layers in layered compounds, which lays a foundation for us to obtain the anisotropic κ of non-layered materials.

The high-angle annular dark-field scanning transmission electron microscopy (HAADF-STEM) also proves this unique structural feature (Figure 1d). The measured lattice constants by electron diffraction are $a = 0.875$ nm, $c = 1.402$ nm (Figure S6), which is consistent with our results of single-crystal diffraction data (Table S1). Because of the light atomic mass of S atoms which are not sensitive for STEM method, only Pb and Sn atoms are clearly observed, however, we unambiguously identify the atomic arrangement of the cross section along *b* axis. As illustrated by dotted rectangle in Figure S7, two dioctahedron chain $PbSnS_3$ units with an angle about 60° arrange serially and form a zigzag shape connected at the end and tail.

We investigated the κ of $PbSnS_3$ single crystal by time-domain thermoreflectance (TDTR) along its three principal axes from 200 K to 400 K (Figure 2a). In TDTR, ultrafast laser was separated to two beams, the pump beam, and the probe beam. The pump beam was modulated by certain frequency and heat the sample periodically, and the time-delayed probe beam was used to detect the temperature change at sample surface by the change of reflectance (so called thermoreflectance).[31] By fitting the temperature decay curve to a corresponding thermal model,[32] we obtain the κ of $PbSnS_3$ single crystal along the *a* direction. The κ along *b* and *c* directions were measured using beam-offset TDTR method. We offset pump and probe beams, and the measured full-width half-maximum (FWHM) of out-of-phase signal contain the information of heat diffusion along the offset direction. By fitting the FWHM using beam-offset thermal model, we obtain the κ along *b* and *c* axes.[46–49] Details of the thermal model fitting and uncertainty analysis are explained in the Supporting Information.

We note that $PbSnS_3$ is a highly insulating material, and its electrical behavior cannot be accurately measured with a nanovoltmeter. The data we obtained in the TDTR measurements represent the total thermal conductivity, with electronic thermal conductivity making almost no contribution to it. As shown in Figure 2a, $PbSnS_3$ single crystal

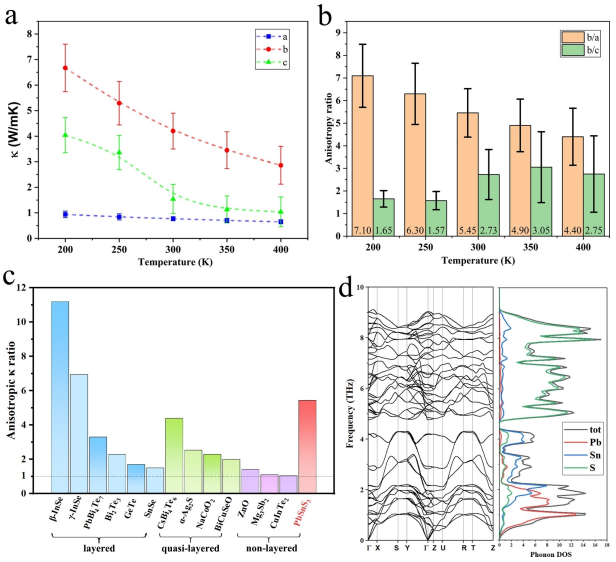

Figure 2. The anisotropic κ of $PbSnS_3$ crystals. a) The temperature-dependent anisotropic κ of $PbSnS_3$ single crystal along different axis by TDTR. b) The κ anisotropy ratios extracted from (a). c) The anisotropic κ ratios of classical thermal functional materials at room temperature. β-InSe[33], γ-InSe[34], $PbBi_4Te_7$[35], Bi_2Te_3[36], GeTe[37], SnSe[38], $CsBi_4Te_6$[39], α-Ag_2S[40], $NaCoO_2$[41], BiCuSeO[42], ZnO[43], Mg_3Sb_2[44], $CuInTe_2$[45]. Data of γ-InSe, BiCuSeO, GeTe, α-Ag_2S, Mg_3Sb_2 and $CuInTe_2$ come from calculated results, while others derive from single crystal samples. d) The calculated phonon dispersions and the corresponding phonon density of states.

possesses a relatively lower κ as 0.77 $W m^{-1} K^{-1}$ at room temperature along *a* axis compared with those along other directions, which shows obvious anisotropy with the ratio κ_b/κ_a up to 7.10 at 200 K and 5.45 at 300 K, indicating a higher ability of heat transmitting along *b* axis (Figure 2b). We compared the anisotropic κ ratio of $PbSnS_3$ with those of other classical thermal functional materials at room temperature (Figure 2c). As a non-layered material, $PbSnS_3$ has a large anisotropy ratio of κ up to 5.45 at room temperature, which surpasses quasi-layered or even some classical layered thermoelectric materials such as BiCuSeO, SnSe, Bi_2Te_3 and GeTe.

In order to explore the origin of the anisotropic κ, we calculated the phonon dispersion of $PbSnS_3$. As seen in Figure 2d, we observe a strong coupling of acoustic branches and the three lowest-frequency optical branches (0.4–1.1 THz). According to the result of phonon density of states (PDOS), those low-frequency phonons dominating heat transport are mainly related to the vibrations of Pb atoms (Figure 2d), calling attention to the influence of the chemical bonds between the Pb and their surrounding atoms. To be specific, three lowest optical branches behave as collective vibrational modes that can be identified as two shear modes and one breathing mode separately (Figure 3a). The two shear modes can correspond to the relative movement of the above-mentioned dioctahedron chain along *b* axis (Figure 3b) and *a* axis (Figure 3c) respectively. The breathing mode (Figure 3d) corresponds to the vibration of these units along *c* direction.

The feature of collective vibrations of a group of atoms frequently arises in layered structure where the vdW gaps break the continuity of chemical bonds. While in $PbSnS_3$, the similar vibration modes come from the maldistribution of chemical bond strength between Pb and S in *ac* plane. The distance between Pb and S atom in the nearest neighbor

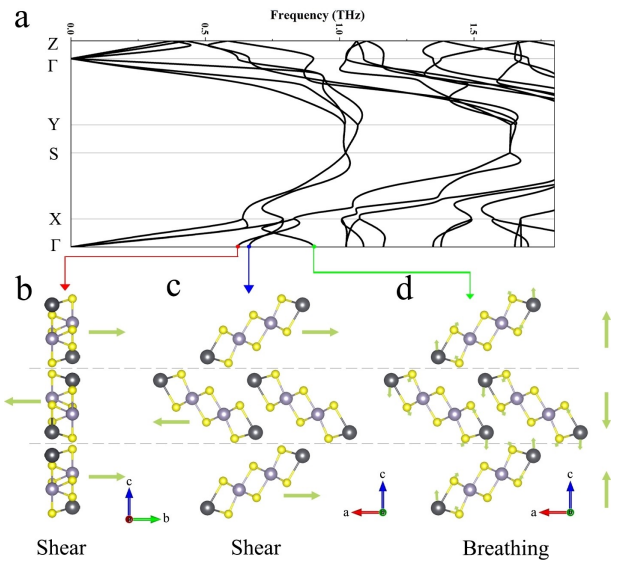

Figure 3. The shear and breathing modes of $PbSnS_3$. a) The low-frequency phonon dispersion spectrum of $PbSnS_3$. b)–d) The Eigen vector of the three lowest-frequency optical phonon modes at Γ point.

dioctahedron chain unit is about 3.1 Å, which weakens the bonding force of Pb–S among different units. The Pb atoms in dioctahedron chain units coordinates with S atoms to form a trigonal pyramidal, leaving a bunch of lone pair electrons locating at the void sites,[29] which can be viewed as isolated weak bonds with neighboring dioctahedron chain units. We analyzed the ELF projected onto the (101) plane at $^1/_4$ and $^3/_4$ b lattice constant where Pb locate (Figure S8). In general, the lone pairs on Pb are toward the void with half to the negative a-axis (slice at $^1/_4$ b) and half to the positive a-axis (slice at $^3/_4$ b). It is evident that the linear density of the lone pairs is highest along the crystal's a-axis. These nonlinear repulsive electrostatic forces among the lone pair electrons can reduce the lattice symmetry and hinder phonon transport. This stereo-unstable state can result in a larger atomic deformation during vibrating compared to the rigid bonds in *b* direction, thus exhibit anharmonicity which is responsible to the reduced κ in *a* direction. It is worth mentioning that the lowest κ is along the direction of shear mode (*a* axis), which is not the common case in layered materials where the lowest κ is along the direction of breathing mode (cross plane). This may arise from that the linear density of the lone pairs is higher along the crystal's *a*-axis than *c*-axis, emphasizing the influence of the directionality of the maldistribution of chemical bond strength on the anisotropic κ.

In order to explain the superior anisotropy of $PbSnS_3$, we evaluated the distinction of bond strength intra and inter the separated units with the -ICOHP of some classical layered materials. As presented by Table S3, in $PbSnS_3$, the -ICOHP of Sn–S bonds in the separated units are much larger than those between the metal and chalcogenide atoms in layered materials, such as Bi–Te, Sn–Se, Ge–Te bonds, where the capped-Pb atoms as electron donors enhance the polarity of the Sn–S bonds and finally lead to the huge distinction of bond strength intra and inter the separated units. Furthermore, it is generally accepted that after hot-pressing the grains of layered materials will be restacked along the (00L) base plane, producing obvious preferred orientation, and maintaining most of the anisotropy. However, this texture should not arise in non-layered $PbSnS_3$ due to the relatively stronger inter-chain Pb–S bond that resist the reorientation under pressure compared with vdW forces. Thus, the absence of the anisotropy of $PbSnS_3$ is reasonable after hot pressing, which is consistent with our experimental results of hot-pressed polycrystalline samples (Figure S9) and prove the non-layered feature of $PbSnS_3$ as well.

We further account for the anisotropic thermal properties by discussing the parameters of phonon transport. Within the framework of the Boltzmann transport equation, we calculated the weighted phase space of three-phonon process in $PbSnS_3$, which is a direct judgment of the number of allowed scattering processes that depends on the phonon dispersions.[50] Apparently, low frequency phonons can provide more momentum and energy-conserving three-phonon scattering channels that affect the κ (Figure S10). Meanwhile, we calculated the relationship between the group velocity and phonon frequency which also exhibit anisotropy (Figure 4a). In the low-frequency region where

most of heat travels, the group velocity of phonon in *b* axis direction (the red points in Figure 4a) obviously dominates, corresponding to the significantly larger κ in *b* axis compared with the other two directions. The TDEP code is also used to calculate the phonon dispersions and group velocity at 400 K (Figure S11 and S12).[51,52] We found that the main temperature-related changes are optical phonons, which have little effect on lattice thermal conductivity.

According to the analysis of Eigen vectors, the lowest-lying optical branch arises from the collective vibration of the dioctahedron chain unit. As the energy increases, vibrations occur between the [SnS_6] octahedron and Pb atoms, as well as between S and Sn atoms. The gap between 4.3–4.8 THz in phonon dispersion is related to the difference in mass between the light S and heavy Pb/Sn atoms, indicating the chemical bond status between the heavy Pb atoms and the neighboring light S atoms in the same chain. Figure 4b presents the calculated lattice differential κ of different directions as a function of phonon frequency, in which the area between the curves and the horizontal axis represents the weight of κ. The peak of differential κ is around 0.5 THz where the coupling of acoustic and optical phonons and the collective vibration occurs. It can also be seen that heat conduction along *b*-direction is predominated comparing to other directions, especially when the phonon frequency above 1 THz.

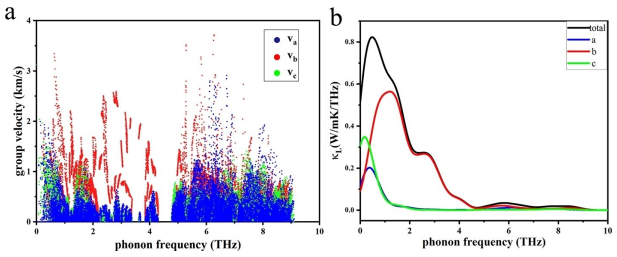

Figure 4. The thermal transport properties of $PbSnS_3$. a) The anisotropic group velocity along *b* axis (the red points) is obviously dominated. b) The calculated κ contributed by different phonon frequency. The contribution along *b* direction is predominated comparing to other directions when the phonon frequency above 1 THz.

Conclusion

Based on the above experimental results as well as the calculations of bond strength and phonon behaviors, we unambiguously propose that the maldistribution of chemical bond strength accounts for the large anisotropic κ in $PbSnS_3$. The lone pair electrons of Pb atoms point to the depth of void formed by sulfur atoms in adjacent dioctahedron chains and weaken the bonding forces among these entireties, resulting in a huge contrast of interaction strength between the intra Sn–S and inter Pb–S atoms which can be even larger than those in some classical layered materials. The maldistribution of chemical bond strength induces the collective vibrations. Besides, due to the tendentious direction of lone pair to the *a*-axes in $PbSnS_3$, the highest sound velocity is along the closely linked *b* axis while the lowest κ is along the direction of shear mode (*a* axis), which is not the common case in layered materials where the lowest κ is along the direction of breathing mode (cross plane). In this mechanism, the maldistribution of chemical bond strength not only maintains the non-layered structure by relatively stronger inter-chain forces than vdW gaps, but also produces separated entireties that hinder the thermal transport among their voids, synergistically causing the high anisotropy ratio of κ in single crystal $PbSnS_3$. As a result, $PbSnS_3$ shows the highest κ anisotropy ratio ever reported in non-layered materials, achieving 7.1 at 200 K and 5.5 at 300 K, respectively.

In summary, we reported a highest anisotropy ratio of κ in non-layered materials up to now, which even surpasses many classical layered materials. Our results show that building maldistribution of chemical bond strength, which originates from the lone pair electrons of low-valence-state p-block elements when they present stereochemically active that repel the closely linked covalent/ionic bonds and hinder the electron sharing in the direction they point to, is an effective and generalizable strategy for obtaining large anisotropic thermal conductivity. The maldistribution of chemical bond strength leads to the collective vibration modes and anisotropic group velocity, which can be combined with advanced structures, such as quantum wells, superlattices, and heterostructures to further improve the anisotropy κ ratios. Additionally, it should be equally effective to both non-layered and layered compounds if maldistribution of chemical bond strength can be introduced into the interior slabs of layered compounds. Therefore, the original concept of maldistribution of chemical bond strength presented in this work not only deepens our understanding of anisotropic thermal properties but also broadens the horizons in design of new materials with large anisotropy κ ratios for application of thermal management.

Acknowledgements

This work was financially supported by the National Key R&D Program of China (2022YFA1203600), the Youth Innovation Promotion Association CAS (Y202092), the CAS Project for Young Scientists in Basic Research (YSBR-070), the Fundamental Research Funds for the Central Universities (WK2340000094), the University Synergy Innovation Program of Anhui Province (GXXT-2020-003, GXXT-2021-022), and National Natural Science Foundation of China (22209167, 12004211, 52161145502), the Tsinghua Shenzhen International Graduate School (QD2021008N, JC2021008), and the Shenzhen Science and Technology Program (RCYX20200714114643187, WDZC20200821100123001).

Conflict of Interest

The authors declare no conflict of interest.

Data Availability Statement

The data that support the findings of this study are available from the corresponding author upon reasonable request.

Keywords: Anisotropy · Non-Layered Materials · Thermal Conductivity

[1] C. Gong, L. Li, Z. Li, H. Ji, A. Stern, Y. Xia, T. Cao, W. Bao, C. Wang, Y. Wang, Z. Q. Qiu, R. J. Cava, S. G. Louie, J. Xia, X. Zhang, *Nature* **2017**, *546*, 265–269.

[2] Y. Deng, Y. Yu, Y. Song, J. Zhang, N. Z. Wang, Z. Sun, Y. Yi, Y. Z. Wu, S. Wu, J. Zhu, J. Wang, X. H. Chen, Y. Zhang, *Nature* **2018**, *563*, 94–99.

[3] Z. Fei, B. Huang, P. Malinowski, W. Wang, T. Song, J. Sanchez, W. Yao, D. Xiao, X. Zhu, A. F. May, W. Wu, D. H. Cobden, J.-H. Chu, X. Xu, *Nat. Mater.* **2018**, *17*, 778–782.

[4] J. Cenker, B. Huang, N. Suri, P. Thijssen, A. Miller, T. Song, T. Taniguchi, K. Watanabe, M. A. McGuire, D. Xiao, X. Xu, *Nat. Phys.* **2021**, *17*, 20–25.

[5] C. Liu, X. Yan, D. Jin, Y. Ma, H.-W. Hsiao, Y. Lin, T. M. Bretz-Sullivan, X. Zhou, J. Pearson, B. Fisher, J. S. Jiang, W. Han, J.-M. Zuo, J. Wen, D. D. Fong, J. Sun, H. Zhou, A. Bhattacharya, *Science* **2021**, *371*, 716–721.

[6] A. F. Santander-Syro, O. Copie, T. Kondo, F. Fortuna, S. Pailhès, R. Weht, X. G. Qiu, F. Bertran, A. Nicolaou, A. Taleb-Ibrahimi, P. Le Fèvre, G. Herranz, M. Bibes, N. Reyren, Y. Apertet, P. Lecoeur, A. Barthélémy, M. J. Rozenberg, *Nature* **2011**, *469*, 189–193.

[7] R. Chaudhuri, S. J. Bader, Z. Chen, D. A. Muller, H. G. Xing, D. Jena, *Science* **2019**, *365*, 1454–1457.

[8] D. C. Vaz, P. Noël, A. Johansson, B. Göbel, F. Y. Bruno, G. Singh, S. McKeown-Walker, F. Trier, L. M. Vicente-Arche, A. Sander, S. Valencia, P. Bruneel, M. Vivek, M. Gabay, N. Bergea, L. F. Baumberger, H. Okuno, A. Barthélémy, A. Fert, L. Vila, I. Mertig, J. P. Attané, M. Bibes, *Nat. Mater.* **2019**, *18*, 1187–1193.

[9] K. I. Uchida, S. Daimon, R. Iguchi, E. Saitoh, *Nature* **2018**, *558*, 95–99.

[10] L. Chen, S. Mankovsky, S. Wimmer, M. A. W. Schoen, H. S. Körner, M. Kronseder, D. Schuh, D. Bougeard, H. Ebert, D. Weiss, C. H. Back, *Nat. Phys.* **2018**, *14*, 490–494.

[11] T. Chen, Y. Chen, A. Kreisel, X. Lu, A. Schneidewind, Y. Qiu, J. T. Park, T. G. Perring, J. R. Stewart, H. Cao, R. Zhang, Y. Li, Y. Rong, Y. Wei, B. M. Andersen, P. J. Hirschfeld, C. Broholm, P. Dai, *Nat. Mater.* **2019**, *18*, 709–716.

[12] K. Hwangbo, Q. Zhang, Q. Jiang, Y. Wang, J. Fonseca, C. Wang, G. M. Diederich, D. R. Gamelin, D. Xiao, J.-H. Chu, W. Yao, X. Xu, *Nat. Nanotechnol.* **2021**, *16*, 655–660.

[13] Y. Pan, C. Le, B. He, S. J. Watzman, M. Yao, J. Gooth, J. P. Heremans, Y. Sun, C. Felser, *Nat. Mater.* **2022**, *21*, 203–209.

[14] S. E. Kim, F. Mujid, A. Rai, F. Eriksson, J. Suh, P. Poddar, A. Ray, C. Park, E. Fransson, Y. Zhong, D. A. Muller, P. Erhart, D. G. Cahill, J. Park, *Nature* **2021**, *597*, 660–665.

[15] M. Zhao, W. Pan, C. Wan, Z. Qu, Z. Li, J. Yang, *J. Eur. Ceram. Soc.* **2017**, *37*, 1–13.

[16] J. Wan, J. Song, Z. Yang, D. Kirsch, C. Jia, R. Xu, J. Dai, M. Zhu, L. Xu, C. Chen, Y. Wang, Y. Wang, E. Hitz, S. D. Lacey, Y. Li, B. Yang, L. Hu, *Adv. Mater.* **2017**, *29*, 1703331.

[17] Q. Yan, M. G. Kanatzidis, *Nat. Mater.* **2022**, *21*, 503–513.

[18] J. He, T. M. Tritt, *Science* **2017**, *357*, eaak9997.

[19] A. J. Minnich, *Nanoscale Microscale Thermophys. Eng.* **2016**, *20*, 1–21.

[20] Y. Cui, M. Li, Y. J. Hu, *J. Mater. Chem. C* **2020**, *8*, 10568–10586.

[21] A. L. Moore, L. Shi, *Mater. Today* **2014**, *17*, 163–174.

[22] O. I. Kalaoglu-Altan, B. K. Kayaoglu, L. Trabzon, *iScience* **2022**, *25*, 103825.

[23] S. Shen, A. Henry, J. Tong, R. Zheng, G. Chen, *Nat. Nanotechnol.* **2010**, *5*, 251–255.

[24] X. J. Wang, V. Ho, R. A. Segalman, D. G. Cahill, *Macromolecules* **2013**, *46*, 4937–4943.

[25] G.-H. Kim, D. Lee, A. Shanker, L. Shao, M. S. Kwon, D. Gidley, J. Kim, K. P. Pipe, *Nat. Mater.* **2015**, *14*, 295–300.

[26] L. Liang, J. Zhang, B. G. Sumpter, Q.-H. Tan, P.-H. Tan, V. Meunier, *ACS Nano* **2017**, *11*, 11777–11802.

[27] G. Pizzi, S. Milana, A. C. Ferrari, N. Marzari, M. Gibertini, *ACS Nano* **2021**, *15*, 12509–12534.

[28] U. v. Alpen, J. Fenner, E. Gmelin, *Mater. Res. Bull.* **1975**, *10*, 175–180.

[29] M. Bletskan, *Semicond. Phys. Quantum Electron. Optoelectron.* **2015**, *18*, 12–19.

[30] X. Qian, J. Zhou, G. Chen, *Nat. Mater.* **2021**, *20*, 1188–1202.

[31] B. Sun, S. Niu, R. P. Hermann, J. Moon, N. Shulumba, K. Page, B. Zhao, A. S. Thind, K. Mahalingam, J. Milam-Guerrero, R. Haiges, M. Mecklenburg, B. C. Melot, Y.-D. Jho, B. M. Howe, R. Mishra, A. Alatas, B. Winn, M. E. Manley, J. Ravichandran, A. J. Minnich, *Nat. Commun.* **2020**, *11*, 6039.

[32] D. G. Cahill, *Rev. Sci. Instrum.* **2004**, *75*, 5119–5122.

[33] A. Rai, V. K. Sangwan, J. T. Gish, M. C. Hersam, D. G. Cahill, *Appl. Phys. Lett.* **2021**, *118*, 073101.

[34] K. Yuan, X. Zhang, Z. Chang, Z. Yang, D. Tang, *ACS Appl. Energy Mater.* **2022**, *5*, 10690–10701.

[35] L. E. Shelimova, T. E. Svechnikova, P. P. Konstantinov, O. G. Karpinskii, E. S. Avilov, M. A. Kretova, V. S. Zemskov, *Inorg. Mater.* **2007**, *43*, 125–131.

[36] H. J. Goldsmid, *Proc. Phys. Soc. London Sect. B* **1956**, *69*, 203–209.

[37] Đ. Dangić, O. Hellman, S. Fahy, I. Savić, *npj Comput. Mater.* **2021**, *7*, 57.

[38] L. D. Zhao, S. H. Lo, Y. Zhang, H. Sun, G. Tan, C. Uher, C. Wolverton, V. P. Dravid, M. G. Kanatzidis, *Nature* **2014**, *508*, 373–377.

[39] D.-Y. Chung, S. D. Mahanti, W. Chen, C. Uher, M. G. Kanatzidis, *MRS Online Proc. Libr.* **2003**, *793*, 206–213.

[40] W. X. Zhou, D. Wu, G. Xie, K. Q. Chen, G. Zhang, *ACS Omega* **2020**, *5*, 5796–5804.

[41] K. Fujita, T. Mochida, K. Nakamura, *Jpn. J. Appl. Phys.* **2001**, *40*, 4644–4647.

[42] S. Kumar, U. Schwingenschlogl, *Phys. Chem. Chem. Phys.* **2016**, *18*, 19158–19164.

[43] P. Jiang, X. Qian, R. Yang, *Rev. Sci. Instrum.* **2017**, *88*, 074901.

[44] J. Zhang, L. Song, M. Sist, K. Tolborg, B. B. Iversen, *Nat. Commun.* **2018**, *9*, 4716.

[45] Y. H. Li, J. Y. Liu, X. Y. Wang, J. W. Hong, *Appl. Phys. Lett.* **2021**, *119*, 243901.

[46] B. Sun, Y. K. Koh, *Rev. Sci. Instrum.* **2016**, *87*, 064901.

[47] J. P. Feser, J. Liu, D. G. Cahill, *Rev. Sci. Instrum.* **2014**, *85*, 104903.

[48] B. Sun, X. Gu, Q. Zeng, X. Huang, Y. Yan, Z. Liu, R. Yang, Y. K. Koh, *Adv. Mater.* **2017**, *29*, 1603297.

[49] B. Sun, G. Haunschild, C. Polanco, J. Z. J. Ju, L. Lindsay, G. Koblmüller, Y. K. Koh, *Nat. Mater.* **2019**, *18*, 136–140.

[50] W. Li, N. Mingo, *Phys. Rev. B* **2015**, *91*, 144304.

[51] O. Hellman, P. Steneteg, I. A. Abrikosov, S. I. Simak, *Phys. Rev. B* **2013**, *87*, 104111.

[52] O. Hellman, I. A. Abrikosov, S. I. Simak, *Phys. Rev. B* **2011**, *84*, 180301.

Manuscript received: March 1, 2023
Accepted manuscript online: May 4, 2023
Version of record online: May 19, 2023